J. Fluid Mech. (2017), *vol.* 822, R3, doi:10.1017/jfm.2017.324

JFM RAPIDS
journals.cambridge.org/rapids

The onset of turbulent rotating dynamos at the low magnetic Prandtl number limit

Kannabiran Seshasayanan[1], **Vassilios Dallas**[1,2] **and Alexandros Alexakis**[1,†]

[1]Laboratoire de Physique Statistique, École Normale Supérieure, CNRS, Université Pierre et Marie Curie, Université Paris Diderot, Paris 75005, France

[2]Department of Applied Mathematics, University of Leeds, Leeds LS2 9JT, UK

(Received 15 March 2017; revised 8 May 2017; accepted 10 May 2017;
first published online 2 June 2017)

We demonstrate that the critical magnetic Reynolds number Rm_c for a turbulent non-helical dynamo in the limit of low magnetic Prandtl number Pm (i.e. $Pm = Rm/Re \ll 1$) can be significantly reduced if the flow is subjected to global rotation. Even for moderate rotation rates the required energy injection rate can be reduced by a factor of more than 10^3. This strong decrease in the onset is attributed to the transfer of energy to the large scales, forming a large-scale condensate, and the reduction in the turbulent fluctuations that cause the flow to have a much larger cutoff length scale than in a non-rotating flow of the same Reynolds number. The dynamo thus behaves as if it is driven just by the large scales that act as a laminar flow (i.e. it behaves as a high Pm dynamo) even though the actual Reynolds number is much higher than the magnetic Reynolds number (i.e. low Pm). Our finding thus points to a new paradigm for the design of new experiments on liquid metal dynamos.

Key words: dynamo theory, geodynamo, rotating turbulence

1. Introduction

The existence of planetary and stellar magnetic fields is attributed to the dynamo instability, the mechanism by which a background turbulent flow spontaneously generates a magnetic field by the constructive refolding of magnetic field lines (Moffatt 1978). Many efforts have been made by several experimental groups to reproduce the dynamo instability in the laboratory using liquid metals (Gailitis *et al.* 2001; Stieglitz & Mueller 2001; Shew & Lathrop 2005; Nornberg *et al.* 2006; Monchaux *et al.* 2007; Giesecke *et al.* 2012). However, so far, unconstrained dynamos driven just by turbulent flows have not been achieved in the laboratory. Successful experimental dynamos rely either on constraining the flow or using ferromagnetic

† Email address for correspondence: alexakis@lps.ens.fr

materials. One of the major challenges to achieving a liquid metal dynamo is the large energy injection rate required to reach the dynamo onset, which is determined by the magnetic Reynolds number $Rm = UL/\eta$ (where U is the r.m.s. velocity, L is the domain size and η is the magnetic diffusivity), which should be larger than a critical value Rm_c. The low value of the magnetic Prandtl number $Pm \equiv \nu/\eta \sim 10^{-5}$ of liquid metals (where ν is the viscosity) implies that the required Reynolds number $Re = UL/\nu = Rm/Pm$ must be very large. The energy injection rate ϵ is proportional to the cubic power of Re, which makes the dynamo onset extremely costly (in energy consumption) to reach in the laboratory. Given that technical constraints limit the size L of laboratory experiments on liquid metal to be no more than a couple of metres, the magnetic diffusivity of liquid sodium is $\eta \simeq 10^{-1}$ m^2 s^{-1} and its density $\rho \simeq 10^3$ kg m^{-3}, we arrive at an energy consumption rate larger than 100 kW assuming $Rm_c \simeq 50$, which is approximately the critical Reynolds number in the constrained dynamos mentioned above (see Pétrélis, Mordant & Fauve 2007). The VKS dynamo, for example, consumed 300 kW at its peak (Monchaux *et al.* 2007). This large required size and the large energy consumption rate limit dynamo experiments to laboratories of industrial size. Note that a reduction of Rm_c even by a factor of 2, i.e. $Rm_c \simeq 25$, reduces this consumption rate to $\sim$10 kW, which is attainable in small-scale laboratories.

From the other side, numerical simulations in the last decade have been able to reach high enough Reynolds numbers to study the dependence of Rm_c as the low Pm limit is approached (Mininni & Montgomery 2005; Ponty *et al.* 2005; Iskakov *et al.* 2007). It was shown that as Re was increased the turbulent fluctuations prevented the dynamo instability, resulting in a value of Rm_c much larger than that of organized laminar flows. The value of Rm_c was shown to increase monotonically for values of Pm around 1, but finally for high enough values of Re (low enough Pm) a finite value of Rm_c was reached independent of Re. This finite value is the turbulent critical magnetic Reynolds number defined as $Rm_c^{turb} \equiv \lim_{Re\to\infty} Rm_c$. Different values of Rm_c^{turb} were obtained for the different flows under study, implying that this number is not universal and that the flows can be optimized to reduce Rm_c^{turb}. This was performed in Sadek, Alexakis & Fauve (2016) by varying the forcing length scale.

In this work we demonstrate that rotation can be used to reduce the dynamo threshold Rm_c^{turb}. Rotation is recognized as one of the key elements that determines the main characteristics of the resulting flows and magnetic fields of planets and stars (Proctor & Gilbert 1994). This is confirmed by observations over the last decade, which have measured the magnetic activity of stars as a function of their rotation period (Reiners, Basri & Browning 2009; Morin *et al.* 2010). It has also been argued that rotation can reduce the dynamo onset (Christensen & Aubert 2006). At fast rotation rates variations along the axis of rotation are suppressed, rendering the flow quasi-2-D in the sense that the flow varies weakly along the direction of rotation while retaining all three velocity components (Alexakis 2015; Dallas & Tobias 2016), a situation referred to in the literature as 2.5-dimensional (2.5-D) flow. These 2.5-D flows have been shown to be effective dynamos (Smith & Tobias 2004; Seshasayanan & Alexakis 2016*a*,*b*). The fact that turbulent fluctuations inhibit the dynamo instability while more organized flows reduce the dynamo threshold (Tobias & Cattaneo 2008*a*,*b*; Tobias, Cattaneo & Boldyrev 2011) indicates that background rotation can provide an efficient way to suppress fluctuations and optimize the flow so that the value of Rm_c^{turb} is reduced. In this work, we demonstrate that this is indeed the case. The effort to achieve the dynamo onset in rotating turbulent flows is modest in comparison to that in non-rotating turbulent flows, with the columnar vortices playing a key role in the spontaneous generation of the magnetic field.

2. Numerical set-up

In this paper we study the kinematic dynamo problem in a rotating frame of reference. Thus, the governing equations involved in this study are

$$\partial_t \boldsymbol{u} + \boldsymbol{u}\cdot\boldsymbol{\nabla}\boldsymbol{u} = -\frac{1}{\rho}\boldsymbol{\nabla} p - 2\boldsymbol{\Omega}\times\boldsymbol{u} + \nu\Delta\boldsymbol{u} + \boldsymbol{f}, \tag{2.1}$$

$$\partial_t \boldsymbol{B} = \boldsymbol{\nabla}\times(\boldsymbol{u}\times\boldsymbol{B}) + \eta\Delta\boldsymbol{B}, \tag{2.2}$$

where $\boldsymbol{u}$ and $\boldsymbol{B}$ are the velocity and the magnetic field respectively with $\boldsymbol{\nabla}\cdot\boldsymbol{u} = \boldsymbol{\nabla}\cdot\boldsymbol{B} = 0$, ρ is the mass density and p is the pressure. The rotation $\boldsymbol{\Omega} = \Omega\hat{\boldsymbol{e}}_z$ is applied along the z-direction. We integrate these equations numerically in a cubic periodic box of length $2\pi L$ using the pseudo-spectral code GHOST (Mininni *et al.* 2011) with a fourth-order Runge–Kutta scheme for the time advancement and the 2/3 de-aliasing rule. The body force is taken to be a 2.5-D non-helical Roberts flow, $\boldsymbol{f} = f_0(\cos(k_f y), \sin(k_f x), \cos(k_f y) + \sin(k_f x))$. Since we are interested in optimizing the flow to reduce the energy consumption in dynamo experiments, we define the non-dimensional parameters in terms of the energy injection/dissipation rate in the system measured by $\epsilon = \nu\langle|\boldsymbol{\nabla}\boldsymbol{u}|^2\rangle$, where $\langle\cdot\rangle$ denotes volume and time average. The non-dimensional parameters in terms of ϵ are the Reynolds number $Re = (\epsilon/k_f)^{1/3}/(k_f\nu)$, the magnetic Reynolds number $Rm = (\epsilon/k_f)^{1/3}/(k_f\eta)$ and the Rossby number $Ro = (\epsilon/k_f)^{1/3}k_f/(2\Omega)$. With this choice of non-dimensionalization Rm_c^{turb} can be related directly to the power ϵ_c required to obtain a dynamo by $\epsilon_c = \rho(2\pi L)^3 k_f^4\eta^3(Rm_c^{turb})^3$. To recover other definitions based on the r.m.s. velocity $U = \langle|\boldsymbol{u}^2|\rangle^{1/2}$ of the flow, $Re_U = U/(k_f\nu)$ and $Ro_U = Uk_f/(2\Omega)$, we provide the dependence of ϵ and U on the control parameters of the system in figure 1(*a*,*b*) and their asymptotic values in table 1.

We are interested in different limits of the parameters in this problem. To model the limit $Re \gg 1$ (or the limit $Pm \ll 1$) we also use hyperviscosity where the Laplacian in the Navier–Stokes equation (2.1) is changed to Δ^4. The use of hyperviscosity assumes that the large scales do not depend on the exact mechanism by which energy is dissipated in the small scales, and thus in principle it should always be compared to the results of large Re simulations.

The other limit we would like to reach is the fast rotating limit $Ro \ll 1$, in which the flow becomes 2.5-D (Gallet 2015). In this case the velocity field becomes invariant along the axis of rotation, and its evolution reduces to the 2-D Navier–Stokes equation for the horizontal components $\boldsymbol{u}_{2D}$ and an advection diffusion equation for the vertical component u_z:

$$\partial_t \boldsymbol{u}_{2D} + \boldsymbol{u}_{2D}\cdot\boldsymbol{\nabla}\,\boldsymbol{u}_{2D} = -\boldsymbol{\nabla}P + \nu\nabla^2\boldsymbol{u}_{2D} + \boldsymbol{f}_{2D}, \tag{2.3}$$

$$\partial_t u_z + \boldsymbol{u}_{2D}\cdot\boldsymbol{\nabla}\,u_z = +\nu\nabla^2 u_z + f_z. \tag{2.4}$$

The magnetic field in this case can be expressed in the form $\boldsymbol{B} = \boldsymbol{b}(x, y, t)\mathrm{e}^{\mathrm{i}k_z z}$ due to the invariance of the flow along the z-direction, where $\boldsymbol{b}$ is a three-component complex vector field. Each k_z-mode evolves independently and the induction equation in this case reads

$$\partial_t\boldsymbol{b} + \boldsymbol{u}_{2D}\cdot\boldsymbol{\nabla}\boldsymbol{b} + u_z\mathrm{i}k_z\boldsymbol{b} = \boldsymbol{b}\cdot\boldsymbol{\nabla}\boldsymbol{u} + \eta(\Delta - k_z^2)\boldsymbol{b}. \tag{2.5}$$

Then, the divergence-free condition $\boldsymbol{\nabla}\cdot\boldsymbol{B} = 0$ for each magnetic mode gives

$$\partial_x b_x(x, y, t) + \partial_x b_y(x, y, t) = -\mathrm{i}k_z b_z(x, y, t). \tag{2.6}$$

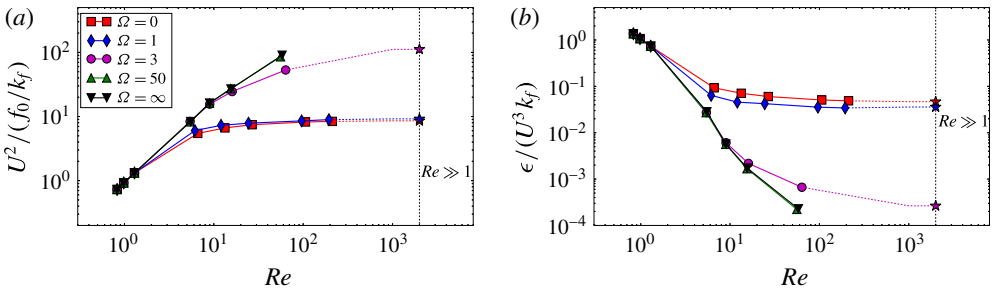

FIGURE 1. The normalized total velocity squared $U^2/(f_0/k_f)$ (a) and the normalized dissipation rate $\epsilon/(U^3 k_f)$ (b) as functions of the Reynolds number Re for different values of the rotation rate as mentioned in the legend. The points denoted by ★ at $Re = 2000$ denote hyperviscosity runs.

Ω	Ro	Re	Ro_U	Re_U	N	Rm_c^{turb}
0	∞	210	∞	580	512	23.6
1	1	200	3	600	512	34.9
3	0.21	64	2.4	720	512	1.81
50	0.011	55	0.18	920	256	—
∞	0	60	0	950	2048	—

TABLE 1. Numerical parameters of the simulations. For all runs $f_0 = 1$, $L = 1$ and $k_f = 4$. N denotes the grid size. The reported values are for the largest values of Re (regular viscosity); Rm_c^{turb} is based on the hyperviscous runs. $\Omega = \infty$ corresponds to the 2.5-D simulations.

In this limit we follow only the $k_z = 1$ mode, which corresponds to the largest mode in our cubic domain and was found to be the most unstable mode (Smith & Tobias 2004; Seshasayanan & Alexakis 2016*b*). The range of the parameters used can be found in table 1.

3. Results

We first describe the effect of rotation on the flow. Rotation affects the velocity field through the Coriolis term. At low Re the flow is laminar and Ω does not modify the velocity field because the laminar flow is invariant along the direction of rotation. As we increase Re beyond a threshold the flow becomes turbulent, varying along all three directions, and hence the effect of Ω becomes more important.

For $\Omega \lesssim 1$, the effect of rotation is not dominant and the underlying flow is not far away from 3-D isotropic turbulence (compared to the cases with $\Omega \geqslant 3$). The total energy U^2 normalized by f_0/k_f and the normalized dissipation rate $\epsilon/(U^3 k_f)$ reach asymptotic values for $Re \to \infty$ as shown in figure 1. These asymptotic values match those obtained by the hyperviscous simulations, which are denoted by star symbols ★, and they are connected with the rest of the data set by dashed lines. This is the classical Kolmogorov turbulence where the large-scale quantities become independent of viscosity at large Re, and all the injected energy cascades via the nonlinearities to the small scales, where it is dissipated at a finite rate (Frisch 1995).

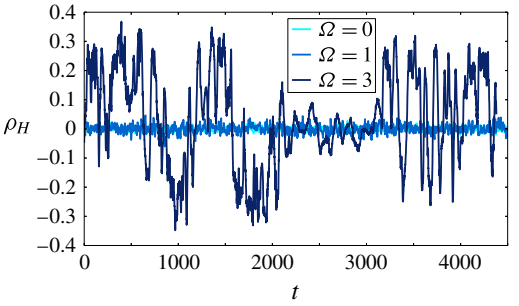

FIGURE 2. Relative helicity ρ_H as a function of time t for different values of Ω mentioned in the legend. Darker shades of blue correspond to larger values of Ω.

For $\Omega = 3$ the flow becomes anisotropic with lesser fluctuations along the z-direction. There is an inverse cascade present in the system, which forms condensates. The growth of the condensate saturates when the counter-rotating vortex locally cancels the effect of global rotation for $U \sim \Omega L$ (Bartello, Métais & Lesieur 1994; Alexakis 2015). The normalized dissipation rate $\epsilon/(U^3 k_f)$ approaches an asymptote but at a much smaller value than in the non-rotating case. For larger rotation rates $\Omega = 50$ and $\Omega = \infty$ saturation comes from viscous forces and $\epsilon/(U^3 k_f)$ decreases with Re. An Re-independent scaling of the $\Omega = 50$ case is also expected at large values of Re where a condensate of amplitude $U \sim \Omega L$ is reached. However, the realization of this behaviour at this large value of Ω is not possible even with hyperviscous runs. Furthermore the 2.5-D runs ($\Omega = \infty$) will saturate due to viscous forces at high amplitudes inversely proportional to viscosity. For these reasons we do not investigate the $\Omega = 50$ and $\Omega = \infty$ runs with hyperviscosity.

Another quantity that is important for large-scale dynamo action is the helicity $H = \langle \boldsymbol{u} \cdot \boldsymbol{\omega} \rangle$ where $\boldsymbol{\omega} = \boldsymbol{\nabla} \times \boldsymbol{u}$ is the vorticity of the flow. Figure 2 shows the normalized helicity $\rho_H = H/(\|\boldsymbol{u}\| \|\boldsymbol{\omega}\|)$ as a function of time for different values of Ω (here $\| \cdot \|$ denotes the L_2 norm). As we can see for $\Omega = 3$, we observe much larger fluctuations of ρ_H whose average over time is zero. Note that the time scale of the fluctuations is much longer than the eddy turnover time scale $L/U \simeq 0.2$. These fluctuations are due to the formation of the condensate (Dallas & Tobias 2016). At small Ω the helicity fluctuations are governed by the small scales, for which the eddy turnover time is very short; for large Ω the helicity fluctuation is governed by the $k_z = 0$ mode, which fluctuates over a much longer time scale. We note that when a condensate forms, most of the energy is concentrated in the largest scales and thus there is no scale separation that would allow us to interpret our dynamo results in terms of an α dynamo (Moffatt 1978).

A priori we do not know whether the transition from a flow with no inverse cascade to a flow with an inverse cascade will decrease the dynamo threshold. To look at the effect of rotation on a dynamo we need to solve for the evolution of the magnetic field. To calculate Rm_c we run simulations of the same flow (same Re and Ro) but with different values of Rm. Rm_c was determined by linear interpolation of the growth rate between runs with a dynamo (positive growth rate) and runs without (negative growth rate). We then repeat the runs for larger values of Re, thus approaching the low Pm limit. Figure 3 shows the critical Reynolds number Rm_c as a function of Re for different values of Ω. The cases of $\Omega = 0$ and 1 display similar behaviour to other studies of non-rotating flows (Mininni & Montgomery 2005;

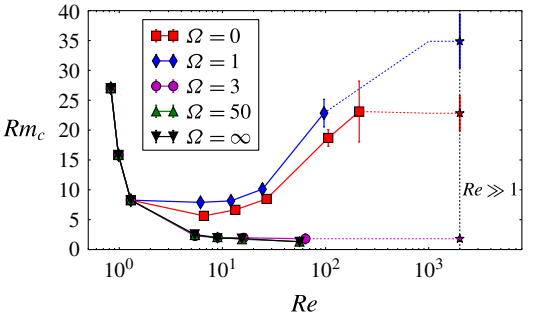

FIGURE 3. Critical magnetic Reynolds number Rm_c as a function of Re for different values of Ω shown in the legend. The points denoted by ★ at $Re = 2000$ denote hyperviscosity runs.

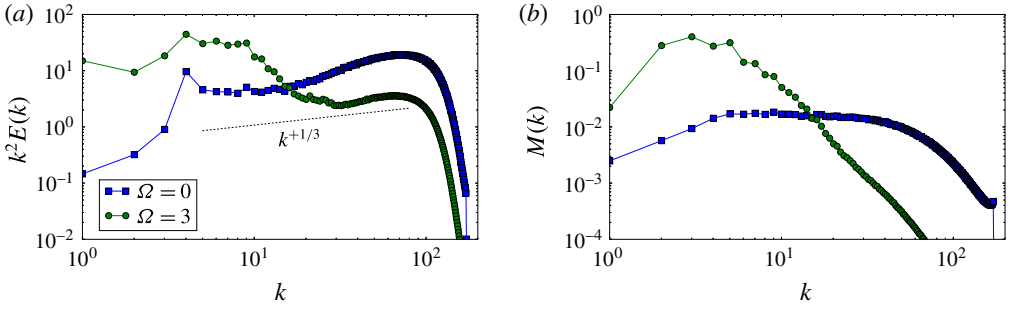

FIGURE 4. (*a*) Compensated kinetic energy spectra $k^2E(k)$ and (*b*) magnetic energy spectra for the two different cases of $\Omega = 0$ and 3 for the hyperviscous runs (i.e. $Pm \ll 1$).

Ponty *et al.* 2005; Iskakov *et al.* 2007) in which Rm_c initially increases with Re, until it begins to become constant at large Re. For $\Omega = 1$ the asymptotic value Rm_c^{turb} is larger than the $\Omega = 0$ case, expressing an initial hindering effect for the dynamo by rotation. For $\Omega \geqslant 3$, however, we see a much lower threshold for the dynamo instability and no such increase due to turbulence is observed. In fact the threshold for $\Omega = 3$ appears no different to that for $\Omega = \infty$, implying that the destructive effect of the 3-D turbulent fluctuations on the dynamo has already disappeared. The ratio between Rm_c^{turb} for the case of $\Omega = 0$ and that for $\Omega = 3$ for the hyperviscous runs is approximately $\sim$12. The injected power ϵ scales like $(Rm_c^{turb})^3$, implying a reduction in the power required for a dynamo instability by a factor of 2×10^3 between $\Omega = 0$ and 3 and a factor of 8×10^3 between $\Omega = 1$ and 3 (see figure 3).

To decipher the reason behind this drop in Rm_c^{turb} at $\Omega = 3$ we display in figure 4(*a*) the enstrophy spectra $k^2E(k)$ for $\Omega = 0$ and $\Omega = 3$ obtained from the hyperviscous runs. Large enstrophy implies a larger stretching rate of the magnetic field lines (although not necessarily constructive). For $\Omega = 0$ a behaviour close to Kolmogorov type is observed, with the enstrophy spectrum $k^2E(k)$ increasing with k after the forcing scale $k_f = 4$. The strongest stretching rate is thus clearly at the small incoherent scales. In contrast, for $\Omega = 3$ the enstrophy spectrum $k^2E(k)$ is decreasing with k. Only at the smallest scales does $k^2E(k)$ start to increase again. Thus, the small-scale fluctuations are suppressed and the dominant stretching rate u_ℓ/ℓ is restricted to the large coherent scales. Figure 5(*b*) shows the vertical vorticity field ω_z for $\Omega = 3$,

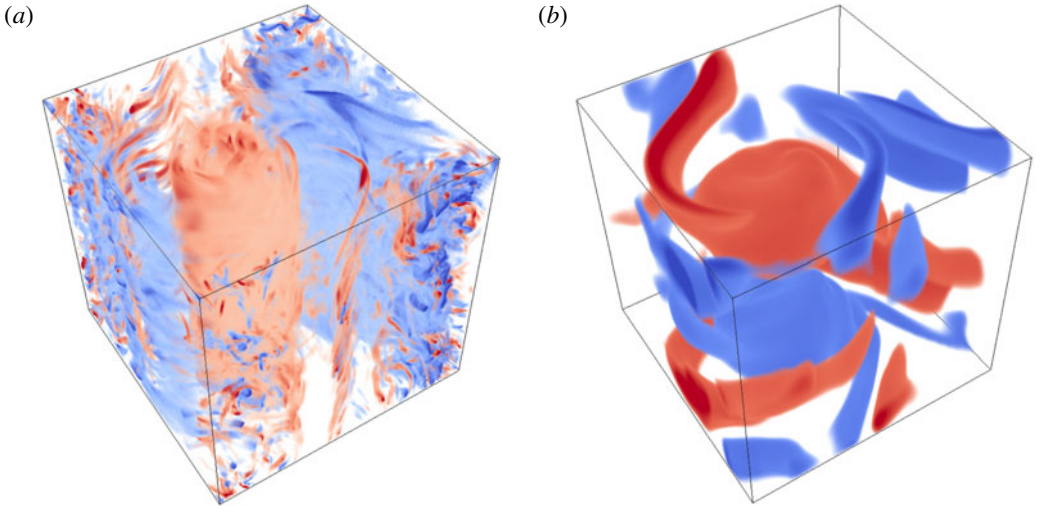

FIGURE 5. (*a*) Colour plot of the vertical vorticity ω_z. (*b*) Vertical current j_z. Red corresponds to positive (co-rotating) values and blue to negative (counter-rotating) values. Both panels have $\Omega = 3$, $Re \approx 60$, $Pm = 0.0375$ and are extracted at the same time.

displaying a strong coherent co-rotating vortex aligned with the global rotation and a counter-rotating vortex responsible for the energy cascade to small scales. Note that the same structure is observed in a flow driven by a Taylor–Green forcing (Alexakis 2015) and in rotating convection (Guervilly, Hughes & Jones 2014). Thus, this structure is not related to the particular choice of forcing used. The dynamo thus behaves as if it is driven just by the organized large scales that act as a laminar flow (i.e. it behaves similarly to a high *Pm* dynamo) even though the actual Reynolds number is much higher than the magnetic Reynolds number (i.e. low *Pm*).

This suppression of small-scale fluctuations, however, is not due to a dissipative mechanism since the Coriolis term is not dissipative and thus does not lead to an extra cost in energy injection.

The magnetic energy spectra for *Rm* close to the onset (i.e. at the kinematic phase of the dynamo) are shown in figure 4(*b*). For the case of $\Omega = 0$ the magnetic energy spectrum is almost flat with an exponential decay at high wavenumbers. The unstable eigenmode (not shown here) takes the form of thin filamentary structures. On the other hand, for $\Omega = 3$ the magnetic energy spectrum decreases fast with k. The peak of the magnetic energy is at the forcing scale ($k_f = 4$), while the energy of the large-scale component ($k = 1$) is more than an order of magnitude smaller. Thus despite the presence of helicity this is not a large-scale dynamo (Ponty & Plunian 2011; Cameron & Alexakis 2016). The structure of the vertical current field j_z from an unstable eigenmode of the dynamo at $\Omega = 3$ is shown in figure 5(*b*). The magnetic field as seen previously in the spectra is present at large scales, with the $k_z = 1$ mode being dominant. Most of the magnetic energy is concentrated along the coherent co-rotating vortex in two oppositely directed spiral flux tubes.

4. Conclusions

The present study shows that global rotation can play a positive role in the dynamo instability by (i) suppressing turbulent fluctuations and (ii) organizing the large scales

in space and time, making them more effective in performing a constructive refolding of the magnetic field lines. These two effects lead the flow to be more efficient in driving the dynamo (at present we cannot be explicit on which of the two effects is more important). This discovery provides a new paradigm for the design of new dynamo experiments that include global rotation.

Our study was performed in an idealized set-up of a triple periodic box. Thus, the question that arises naturally is to what extent these results can carry over to more realistic domains and boundary conditions. Boundaries can delay the inverse cascade (as has been noted in rotating convection (Kunnen *et al.* 2016; Plumley *et al.* 2016)) and can also introduce further dissipation mechanisms in the boundary layers such as Ekman friction. To answer this question, further work needs to be pursued with simulations in more realistic domains. Nevertheless we note that reaching rotation rates in the laboratory that lead to quasi-2-D flows is feasible and has already been achieved in water-tank experiments (Yarom, Vardi & Sharon 2013; Campagne *et al.* 2014). Furthermore, in Campagne *et al.* (2016) the dissipated power in rotating turbulence was directly measured and was shown to decrease by a factor of 10 at the highest rotation examined, compared to the dissipated power in non-rotating turbulence, due to a two-dimensionalization of the flow. At the examined rotation rates no enhancement of the viscous dissipation due to Ekman layers was observed. So, suppressing turbulent fluctuations and decreasing energy dissipation by adding global rotation is indeed feasible experimentally. The additional energy cost of maintaining the rotation is probably minimal compared to the large gain of the order of 10^3 due to the suppression of turbulent fluctuations. Another issue that needs to be considered is the design of the domain and the forcing, which should guarantee that all three velocity components are present, so that the flow becomes 2.5-D and not 2-D. This difficulty can be overcome by the proper design of the forcing mechanism that amplifies all velocity components.

Finally, we note that this result also shows that in fast rotating systems, such as the Earth, the critical magnetic Reynolds number based on the energy injected to sustain a dynamo instability might stay very small, $Rm \sim O(1)$, even at large Reynolds numbers.

Acknowledgements

The authors acknowledge enlightening discussions with S. Fauve. V.D. acknowledges support from the Royal Society and the British Academy of Sciences (Newton International Fellowship, NF140631). The computations were performed using the HPC resources from GENCI-TGCC-CURIE (Project no. x2016056421) and ARC1, part of the High Performance Computing facilities at the University of Leeds, UK.

References

ALEXAKIS, A. 2015 Rotating Taylor–Green flow. *J. Fluid Mech.* **769**, 46–78.

BARTELLO, P., MÉTAIS, O. & LESIEUR, M. 1994 Coherent structures in rotating three-dimensional turbulence. *J. Fluid Mech.* **273**, 1–29.

CAMERON, A. & ALEXAKIS, A. 2016 Fate of alpha dynamos at large *Rm*. *Phys. Rev. Lett.* **117**, 205101.

CAMPAGNE, A., GALLET, B., MOISY, F. & CORTET, P.-P. 2014 Direct and inverse energy cascades in a forced rotating turbulence experiment. *Phys. Fluids* **26** (12), 125112.

CAMPAGNE, A., MACHICOANE, N., GALLET, B., CORTET, P. & MOISY, F. 2016 Turbulent drag in a rotating frame. *J. Fluid Mech.* **794**, R5.

CHRISTENSEN, U. R. & AUBERT, J. 2006 Scaling properties of convection-driven dynamos in rotating spherical shells and application to planetary magnetic fields. *Geophys. J. Intl* **166** (1), 97–114.

DALLAS, V. & TOBIAS, S. M. 2016 Forcing-dependent dynamics and emergence of helicity in rotating turbulence. *J. Fluid Mech.* **798**, 682–695.

FRISCH, U. 1995 *Turbulence: The Legacy of A. N. Kolmogorov*. Cambridge University Press.

GAILITIS, A., LIELAUSIS, O., PLATACIS, E., DEMENT'EV, S., CIFERSONS, A., GERBETH, G., GUNDRUM, T., STEFANI, F., CHRISTEN, M. & WILL, G. 2001 Magnetic field saturation in the Riga dynamo experiment. *Phys. Rev. Lett.* **86**, 3024–3027.

GALLET, B. 2015 Exact two-dimensionalization of rapidly rotating large-Reynolds-number flows. *J. Fluid Mech.* **783**, 412–447.

GIESECKE, A., STEFANI, F., GUNDRUM, T., GERBETH, G., NORE, C. & LORAT, J. 2012 Experimental realization of dynamo action: present status and prospects. In *Solar and Astrophysical Dynamos and Magnetic Activity, Proc. IAU,* vol. 8, pp. 411–416. Cambridge University Press.

GUERVILLY, C., HUGHES, D. W. & JONES, C. A. 2014 Large-scale vortices in rapidly rotating Rayleigh–Bénard convection. *J. Fluid Mech.* **758**, 407–435.

ISKAKOV, A. B., SCHEKOCHIHIN, A. A., COWLEY, S. C., MCWILLIAMS, J. C. & PROCTOR, M. R. E. 2007 Numerical demonstration of fluctuation dynamo at low magnetic Prandtl numbers. *Phys. Rev. Lett.* **98**, 208501.

KUNNEN, R. P. J., OSTILLA-MÓNICO, R., VAN DER POEL, E. P., VERZICCO, R. & LOHSE, D. 2016 Transition to geostrophic convection: the role of the boundary conditions. *J. Fluid Mech.* **799**, 413–432.

MININNI, P. D. & MONTGOMERY, D. C. 2005 Low magnetic Prandtl number dynamos with helical forcing. *Phys. Rev.* E **72**, 056320.

MININNI, P. D., ROSENBERG, D., REDDY, R. & POUQUET, A. 2011 A hybrid MPI–OpenMp scheme for scalable parallel pseudospectral computations for fluid turbulence. *Parallel Comput.* **37** (6), 316–326.

MOFFATT, H. K. 1978 *Magnetic Field Generation in Electrically Conducting Fluids*. Cambridge University Press.

MONCHAUX, R., BERHANU, M., BOURGOIN, M., MOULIN, M., ODIER, P., PINTON, J.-F., VOLK, R., FAUVE, S., MORDANT, N., PÉTRÉLIS, F. *et al.* 2007 Generation of a magnetic field by dynamo action in a turbulent flow of liquid sodium. *Phys. Rev. Lett.* **98**, 044502.

MORIN, J., DONATI, J.-F., PETIT, P., DELFOSSE, X., FORVEILLE, T. & JARDINE, M. M. 2010 Large-scale magnetic topologies of late M dwarfs. *Mon. Not. R. Astron. Soc.* **407**, 2269–2286.

NORNBERG, M. D., SPENCE, E. J., KENDRICK, R. D., JACOBSON, C. M. & FOREST, C. B. 2006 Intermittent magnetic field excitation by a turbulent flow of liquid sodium. *Phys. Rev. Lett.* **97**, 044503.

PÉTRÉLIS, F., MORDANT, N. & FAUVE, S. 2007 On the magnetic fields generated by experimental dynamos. *Geophys. Astrophys. Fluid Dyn.* **101** (3–4), 289–323.

PLUMLEY, M., JULIEN, K., MARTI, P. & STELLMACH, S. 2016 The effects of Ekman pumping on quasi-geostrophic Rayleigh–Bénard convection. *J. Fluid Mech.* **803**, 51–71.

PONTY, Y., MININNI, P. D., MONTGOMERY, D. C., PINTON, J.-F., POLITANO, H. & POUQUET, A. 2005 Numerical study of dynamo action at low magnetic Prandtl numbers. *Phys. Rev. Lett.* **94**, 164502.

PONTY, Y. & PLUNIAN, F. 2011 Transition from large-scale to small-scale dynamo. *Phys. Rev. Lett.* **106**, 154502.

PROCTOR, M. R. E. & GILBERT, A. D. 1994 *Lectures on Solar and Planetary Dynamos*. Cambridge University Press.

REINERS, A., BASRI, G. & BROWNING, M. 2009 Evidence for magnetic flux saturation in rapidly rotating M stars. *Astrophys. J.* **692** (1), 538–545.

SADEK, M., ALEXAKIS, A. & FAUVE, S. 2016 Optimal length scale for a turbulent dynamo. *Phys. Rev. Lett.* **116**, 074501.

SESHASAYANAN, K. & ALEXAKIS, A. 2016*a* Kazantsev model in non-helical 2.5-dimensional flows. *J. Fluid Mech.* **806**, 627–648.

SESHASAYANAN, K. & ALEXAKIS, A. 2016*b* Turbulent 2.5-dimensional dynamos. *J. Fluid Mech.* **799**, 246–264.

SHEW, W. L. & LATHROP, D. P. 2005 Liquid sodium model of geophysical core convection. *Phys. Earth Planet. Inter.* **153**, 136–149.

SMITH, S. G. L. & TOBIAS, S. M. 2004 Vortex dynamos. *J. Fluid Mech.* **498**, 1–21.

STIEGLITZ, R. & MUELLER, U. 2001 Experimental demonstration of a homogeneous two-scale dynamo. *Phys. Fluids* **13** (3), 561–564.

TOBIAS, S. M. & CATTANEO, F. 2008*a* Dynamo action in complex flows: the quick and the fast. *J. Fluid Mech.* **601**, 101–122.

TOBIAS, S. M. & CATTANEO, F. 2008*b* Limited role of spectra in dynamo theory: coherent versus random dynamos. *Phys. Rev. Lett.* **101** (12), 125003.

TOBIAS, S. M., CATTANEO, F. & BOLDYREV, S. 2011 MHD dynamos and turbulence. In *Ten Chapters in Turbulence* (ed. P. A. Davidson, Y. Kaneda & K. R. Sreenivasan), pp. 351–397. Cambridge University Press.

YAROM, E., VARDI, Y. & SHARON, E. 2013 Experimental quantification of inverse energy cascade in deep rotating turbulence. *Phys. Fluids* **25** (8), 085105.